24. Maher, B. A. & Thompson, R. in *Quaternary Climates, Environments and Magnetism* (eds Maher, B. A. & Thompson, R.) 1–48 (Cambridge Univ. Press, Cambridge, UK, 1999).
25. Chapman, M. R. & Shackleton, N. J. Millennial-scale fluctuations in North Atlantic heat flux during the last 150,000 years. *Earth Planet. Sci. Lett.* **159,** 57–70 (1998).
26. Hovan, S. A., Rea, D. K. & Pisias, N. G. Late Pleistocene continental climate and oceanic variability recorded in Northwest Pacific sediments. *Paleoceanography* **6,** 349–370 (1991).
27. DeMenocal, P. B., Ruddiman, W. F. & Pokras, E. M. Influences of high-latitude and low-latitude processes on African terrestrial climate—Pleistocene eolian records from Equatorial Atlantic-Ocean drilling Program Site-663. *Paleoceanography* **8,** 209–242 (1993).

Acknowledgements

We are grateful to Southampton Oceanography Centre for allowing sampling of Core 82PCS01. We also thank K. Miller for picking the foraminifera, and S. Dennis and G. McIntosh for performing oxygen isotope and magnetic analyses, respectively.

Correspondence and requests for materials should be addressed to B.M. (e-mail: b.maher@lancaster.ac.uk).

Delayed triggering of the 1999 Hector Mine earthquake by viscoelastic stress transfer

Andrew M. Freed* & Jian Lin†

* *Department of Terrestrial Magnetism, Carnegie Institution of Washington, Washington DC 20015, USA*
† *Department of Geology and Geophysics, Woods Hole Oceanographic Institution, Woods Hole, Massachusetts 02543 USA*

Stress changes in the crust due to an earthquake can hasten the failure of neighbouring faults and induce earthquake sequences in some cases[1–5]. The 1999 Hector Mine earthquake in southern California (magnitude 7.1) occurred only 20 km from, and 7 years after, the 1992 Landers earthquake (magnitude 7.3). This suggests that the Hector Mine earthquake was triggered in some fashion by the earlier event. But uncertainties in the slip distribution and rock friction properties associated with the Landers earthquake have led to widely varying estimates of both the magnitude and sign of the resulting stress change that would be induced at the location of the Hector Mine hypocentre—with estimates varying from −1.4 bar (ref. 6) to +0.5 bar (ref. 7). More importantly, coseismic stress changes alone cannot satisfactorily explain the delay of 7 years between the two events. Here we present the results of a three-dimensional viscoelastic model that simulates stress transfer from the ductile lower crust and upper mantle to the brittle upper crust in the 7 years following the Landers earthquake. Using viscoelastic parameters that can reproduce the observed horizontal surface deformation following the Landers earthquake, our calculations suggest that lower-crustal or upper-mantle flow can lead to postseismic stress increases of up to 1–2 bar at the location of the Hector Mine hypocentre during this time period, contributing to the eventual occurrence of the 1999 Hector Mine earthquake. These results attest to the importance of considering viscoelastic processes in the assessment of seismic hazard[8–11].

Earthquake triggering relationships have typically been quantified by changes in Coulomb stress occurring coseismically, $\Delta\sigma_f = \Delta\tau + \mu'\Delta\sigma_n$, where $\Delta\tau$ is the change in shear stress in the slip direction of the receiver fault, $\Delta\sigma_n$ is the change in normal stress (tension positive), and μ' is the apparent coefficient of friction incorporating the influence of pore pressure. Numerous studies have shown good correlations between calculated positive coseismic stress changes and the locations of aftershocks[1,2,12–15] as well as triggering of moderate to large earthquakes[2–5,16,17]. For example, the 1933 Long Beach and 1952 Kern County earthquakes were calculated to have increased coseismic stress in the region of the 1971 San Fernando earthquake, which in turn may have increased coseismic stress at the sites of the 1987 Whittier Narrows and 1994 Northridge events[16].

A limitation of the coseismic stress models is that they only consider elastic responses to fault slip, and thus cannot account for delay times in the triggering process. One possible source for postseismic stress changes is viscous relaxation. Previous analyses have shown that viscous flow in the lower crust or upper mantle after a moderate or major earthquake can lead to significant increases in stress and strain in the seismogenic upper crust, causing it eventually to become the main layer storing strains associated with the original rupture[8–11]. Geodetic studies have revealed rapid regional-scale changes in surface deformation following the Landers earthquake[18–22]. Though a host of processes—including fault-zone collapse[19], afterslip[18,20] and poroelastic rebound[23]—may influence postseismic surface deformation, viscous flow in either the lower crust[24,25] or (predominantly) the upper mantle[26] appears to best explain the observed horizontal surface deformation following the Landers earthquake. Although the viscous-upper-mantle model does a better job of explaining the observed vertical surface deformation[26], the viscous-lower-crust model is more consistent with petrological arguments that a felsic lower crust should be closer to its melting point and therefore weaker than a mafic upper mantle[27]. We therefore consider both rheologies in our calculations of postseismic stress changes.

The June 1992 Landers earthquake, moment magnitude M_w = 7.3, was part of an earthquake sequence that began with the April 1992 M_w = 6.1 Joshua Tree preshock and continued with the M_w = 6.2 Big Bear aftershock only a few hours after the Landers rupture[28] (Fig. 1). To investigate the influence of viscous dissipation following the Landers sequence, we developed a three-dimensional, viscoelastic, finite-element model of a portion of the southern California lithosphere (Fig. 2). Our model considers fault slip associated with the Landers sequence in accordance with slip distributions inferred by the combined inversion of strong motion, teleseismic motion and geodetic data[29]. Previous coseismic analyses of the Landers earthquake approximated the complex rupture surface by mapping slip distributions to three or four linear fault segments[1,2,6,7]. Changes in Coulomb stress are, however, sensitive to kinks and jumps in the slip distribution. This is especially true for the Hector Mine hypocentre that is located only 20 km from the region of maximum slip (5–6 m) during the Landers earthquake, where rupture jumped from the Emerson to the Homestead Valley segments[28] (Fig. 1b). To achieve the best possible accuracy of the calculated coseismic stress changes, we therefore mapped the inferred Landers slip distribution onto fault geometry dictated by observed surface breaks[28] (Fig. 2c).

The reasonableness of our Landers slip model is demonstrated by the good correspondence between the calculated coseismic Coulomb stress increases and the observed aftershocks (Fig. 1). Specifically, the model predicts the location of aftershock clusters, which are especially diagnostic of Landers stress changes as opposed to more randomly distributed normal background seismicity. Of particular interest in Fig. 1b is the region of calculated positive coseismic stress change that extends to the northeast of Landers, encompassing a cluster of aftershocks that occurred near the subsequent Hector Mine epicentre. The occurrence of this aftershock cluster implies crustal weakness near the subsequent Hector Mine rupture site, suggesting that even though coseismic stress changes were not sufficient to trigger the Hector Mine earthquake, the triggering threshold was probably close. Reasonable agreement between our Coulomb stress results and aftershock locations is achieved by assuming an apparent friction coefficient in the range $0.2 < \mu' < 0.6$, with $\mu' = 0.4$ for the example shown in Fig. 1. Our

coseismic model is also in reasonable agreement (within 10%) with the magnitude and orientation of coseismic horizontal displacement vectors as determined by GPS (Global Positioning System) and trilateration measurements[29].

A more direct calculation of the influence of the Landers earthquake on the triggering of the subsequent Hector Mine rupture is to

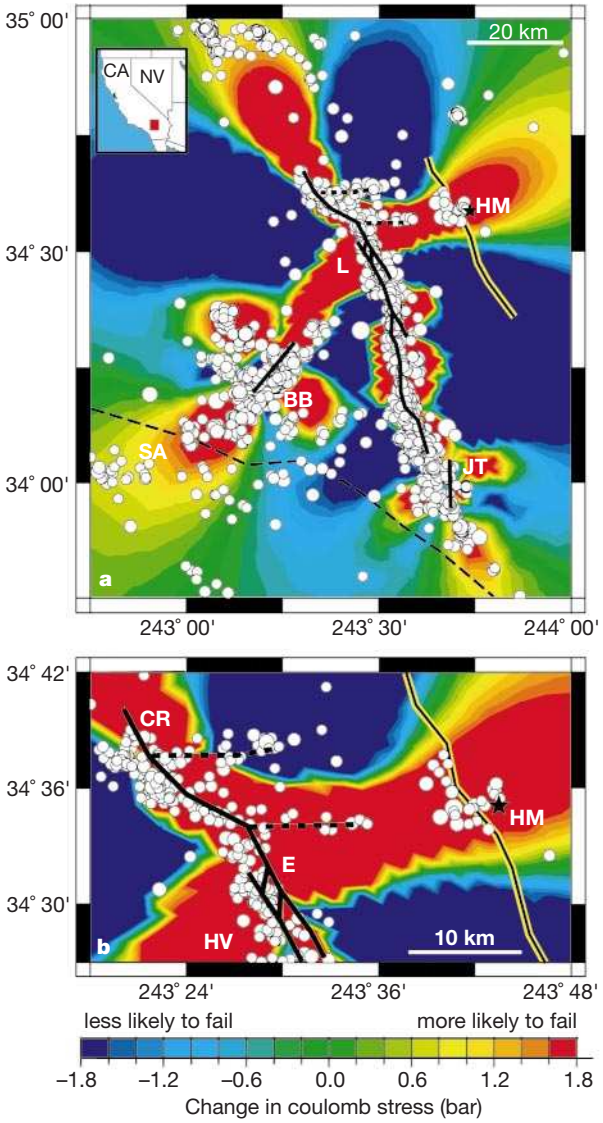

Figure 1 Correspondence between observed aftershocks and calculated coseismic changes in Coulomb stress associated with the 1992 Landers earthquake sequence. **a**, Surface rupture geometry of the 1992 Landers (L), Big Bear (BB) and Joshua Tree (JT) earthquakes (solid black lines) as well as the 1999 Hector Mine (HM) earthquake (black on yellow line) and the San Andreas (SA) fault (dashed line). Hector Mine epicentre is shown by a star. The study region is in southern California (red box in inset). CA, California; NV, Nevada. **b**, Details of the northern portion of the Landers rupture region showing the Camp Rock (CR), Emerson (E), and Homestead Valley (HV) segments. Inferred buried east–west rupture surfaces[28] are shown as dashed lines. Seismicity ($M_w > 3$) shown (white dots) is for a period from the Landers earthquake (28 June 1992) to just before the Hector Mine earthquake (16 October 1999). Background shows the calculated coseismic Coulomb stress changes based on slip of the 1992 Landers earthquake sequence (see text). Regions of positive Coulomb stress changes are shown in red, negative changes are in blue. Receiver fault orientations were calculated considering both the coseismic stresses and a 100-bar regional compressional stress field with its maximum compression axis at N7E[1,2]. The apparent coefficient of friction is $\mu' = 0.4$. All earthquakes are right-lateral strike slip except for the Big Bear earthquake that is left lateral.

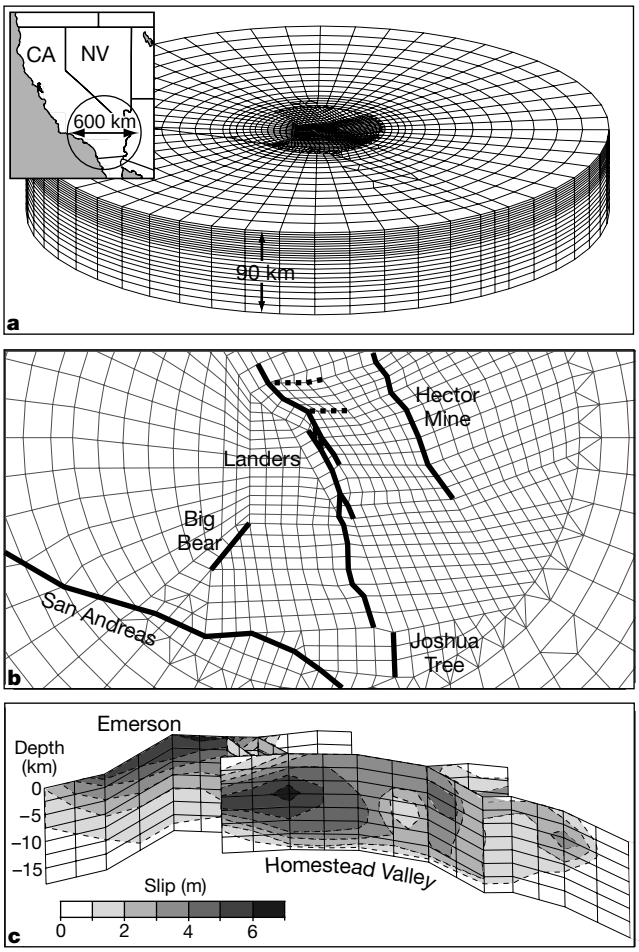

Figure 2 Viscoelastic finite-element model used to calculate coseismic and postseismic Coulomb stress changes associated with the 1992 Landers earthquake sequence. The model (**a**) comprises a cylindrical region of the southern California lithosphere with a diameter of 600 km and a depth of 90 km, centred at the Landers epicentre (inset). The cylindrical shape of the model efficiently minimizes the influence of the distant boundary conditions, which are assumed to be fixed in displacement on the edge and bottom. We used the finite-element code I-deas (see http://www.sdrc.com), a widely used engineering code that we have adapted for use in geodynamical problems. A close-up of the model centre detailing fault geometry is shown in **b**. Modelled slip distribution[29] for the Emerson and Homestead Valley segments of the Landers rupture is shown in **c**. Fault ruptures are modelled explicitly by defining slip between coincident nodes on the predefined rupture surfaces. The crust and mantle are modelled with elastic Young's moduli of 8×10^{10} and 1×10^{11} Pa, respectively, and a Poisson's ratio of 0.25. The model calculates the evolution of Coulomb stress changes associated with the relaxation of viscous lower crust and/or upper mantle. We examine two end-member cases. The first case considers viscous flow in a lower crust layer[25] that lies in the depth range of 18 to 28 km with a viscosity of 5×10^{18} Pa s. The second case considers predominantly viscous flow in the upper mantle[26], for which the lower crust has a viscosity of 1.6×10^{19} Pa s, the top portion of the upper mantle (28–50 km depth) has a viscosity of 8×10^{18} Pa s, and the lower portion of the upper mantle (50–90 km depth) has a viscosity of 5×10^{18} Pa s. Our calculations show that these sets of parameters can satisfactorily reproduce the observed horizontal surface deformation along the USGS Emerson geodetic line[20], with the discrepancies between models and observation $\leq$10%. Our model of viscous lower-crustal flow has a viscosity 5 times that suggested in ref. 25, while for our model of viscous upper-mantle flow, the mantle viscosity below 50 km is twice that suggested in ref. 26. These differences are probably due to differences in the modelled Landers slip distribution, assumed elastic properties, and our fixed boundary at a depth of 90 km. Extending the bottom boundary to a depth of 200 km changes our elastic stress results by less than 0.03 bar.

constrain the receiver faults in the Coulomb modelling to be right-lateral and to be parallel to the observed Hector Mine rupture surface (N20W). The resulting coseismic Coulomb stress changes with respect to this orientation are shown in Fig. 3a, both for the top ground surface and for a cross-sectional view of the model along the Hector Mine rupture surface. These results show that the Hector Mine hypocentre is located near a narrow strip of slightly positive Coulomb stress changes bounded by regions of negative stress changes to the north and south. However, slight changes in the assumed slip distribution and rupture geometry of the Landers earthquake can shift this region of slightly positive stress changes several kilometres to the north or south, resulting in significantly different predictions of positive or negative coseismic stress changes at the Hector Mine hypocentre. This is a major reason for the lack of a consensus[6,7] on the sign and magnitude of the coseismic stress changes at the Hector Mine hypocentre. We calculate the coseismic Coulomb stress changes at the point of the Hector Mine hypocentre to be from −0.2 bar for a relatively high apparent friction ($\mu' = 0.8$) to −0.8 bar for a relatively low apparent friction ($\mu' = 0.2$) (see Fig. 4a for year 1992). Figure 3a displays the case of high apparent friction, as high friction along the Hector Mine rupture zone was inferred from a previous study[7].

Of particular interest to this study is the large lobe of positive coseismic Coulomb stress changes induced in the lower crust and upper mantle by the Landers earthquake (Fig. 3a). This deep region of Coulomb stress increase is primarily driven by significant coseismic slip (5–6 m) between 5 and 12 km depth on the Homestead Valley segment of the Landers rupture zone (Fig. 2c). If either the viscous lower crust or upper mantle is unable to sustain this load following the Landers earthquake, this initial lobe of coseismic Coulomb stress increase must migrate into the upper crust as the lower crust or upper mantle relaxes. For the case of viscous lower-crustal flow, Coulomb stress at the Hector Mine hypocentre is calculated to increase by about 1 bar during the time interval from 1992 to 1999 (Fig. 3b and c). The magnitude of this increase is not very sensitive to the assumed coefficient of friction (Fig. 4a). For the case of viscous upper-mantle flow, Coulomb stress at the Hector Mine hypocentre is calculated to increase by more than 2 bar in the 1992 to 1999 time interval (Fig. 3d and e). This result is also not very sensitive to the assumed friction (Fig. 4b). The calculated post-seismic stress increase at the Hector Mine hypocentre is greater for the viscous upper mantle flow case because the initial reservoir of positive coseismic stress changes was greater in the upper mantle than in the lower crust (Fig. 3a).

In addition to explaining the delayed triggering of the Hector Mine earthquake, postseismic stress changes following the Landers earthquake may also have influenced the spatial extent of the Hector Mine rupture zone. Relaxation of the viscous lower crust (Fig. 3c) and upper mantle (Fig. 3e) is calculated to cause postseismic stress increase over two-thirds and the full length, respectively, of the

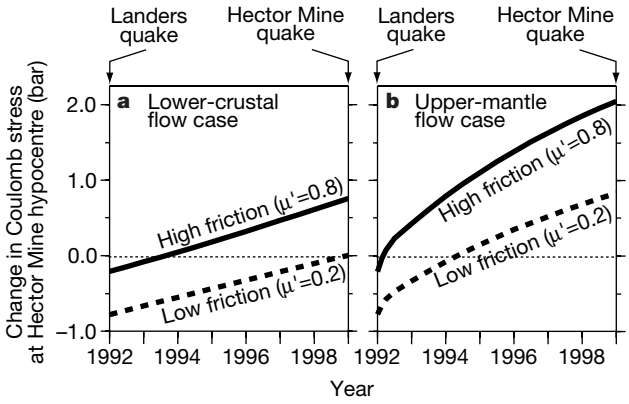

Figure 4 Calculated Coulomb stress changes at the Hector Mine hypocentre as a function of year and assumed friction. **a**, For a model that assumes viscous flow occurs only in the lower crust. **b**, For a model that assumes viscous flow occurs predominantly in the upper mantle. The calculated positive postseismic Coulomb stress changes suggest that the Hector Mine hypocentre was brought closer to failure by post-Landers relaxation processes regardless of the apparent friction or whether viscous flow occurs predominantly in the lower crust or upper mantle.

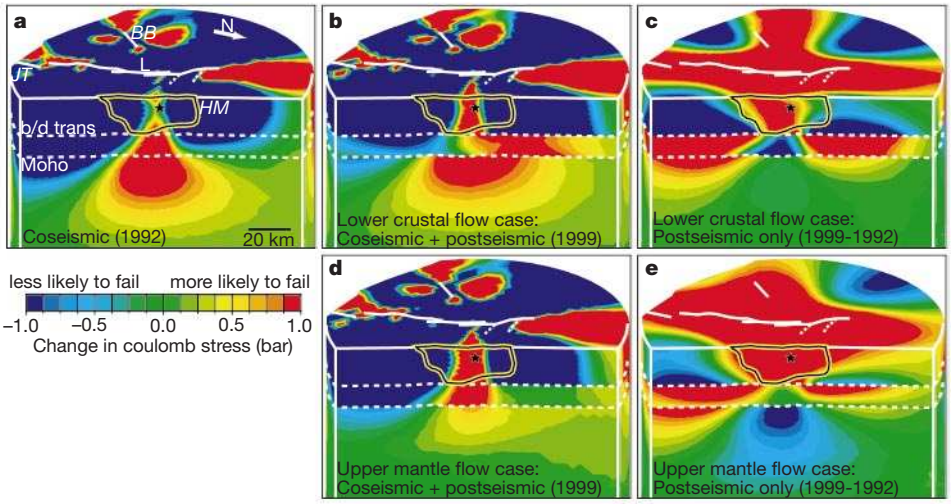

Figure 3 Calculated coseismic and postseismic changes in Coulomb stress associated with the 1992 Landers earthquake sequence. **a**, Calculated coseismic Coulomb stress changes shown both for the top ground surface and for a cross-sectional view of the model along the Hector Mine rupture surface, which is defined by regions of at least 1 m of slip[30] (surface encompassed by the black on yellow line). The Hector Mine hypocentre is shown by a black star. The Joshua Tree (JT), Landers (L) and Big Bear (BB) rupture surfaces are shown as white lines on the top ground surface. The lower crust lies between the brittle/ductile transition (b/d trans) at 18 km depth and the Moho at 28 km depth. The receiver faults are assumed to have the same orientation as the Hector Mine rupture zone (N20W). All calculations shown assume apparent friction $\mu' = 0.8$. **b**, Calculated combined coseismic and 7 years of postseismic Coulomb stress changes if viscous flow occurs predominantly in the lower crust. We note that whereas stress tensors and the displacement field are continuous throughout the entire model in these calculations, the resultant Coulomb stress changes can be very sharp across the brittle/ductile transition and Moho owing to discontinuous viscoelastic properties. **c**, As **b** but for postseismic Coulomb stress changes only. **d**, Calculated combined coseismic and 7 years of postseismic Coulomb stress changes caused by predominantly viscous flow of the upper mantle. **e**, As **d** but for postseismic Coulomb stress changes only.

eventual Hector Mine rupture surface. Meanwhile, for both cases, the net (coseismic plus postseismic) changes in Coulomb stress remained negative at and beyond the distal ends of the Hector Mine rupture surface (Fig. 3b and d). Thus, it is possible that, once triggered, the Hector Mine rupture propagated to the north and south until it encountered these regions of negative net stress changes. Propagation part of the way into these negative-stress regions could be explained by the dynamics of the rupture process, which itself could have increased stress levels at the propagation fronts. Alternatively, the lateral extent of the Hector Mine rupture zone may have been controlled by the mechanical heterogeneity of the crust in the region rather than by the spatial patterns of stress changes. These results attest to the importance of considering viscoelastic processes in the assessment of seismic hazard and its migratory pattern[8–11]. □

Received 18 September 2000; accepted 8 March 2001.

1. Stein, R. S., King, G. C. P. & Lin, J. Change in failure stress on the southern San Andreas fault system caused by the 1992 magnitude = 7.4 Landers earthquake. *Science* **258,** 1328–1332 (1992).
2. King, G. C. P., Stein, R. S. & Lin, J. Static stress changes and the triggering of earthquakes. *Bull. Seismol. Soc. Am.* **84,** 935–953 (1994).
3. Deng, J. & Sykes, L. R. Triggering of 1812 Santa Barbara earthquake by a great San Andreas shock: Implications for future seismic hazards in southern California. *Geophys. Res. Lett.* **23,** 1155–1158 (1996).
4. Harris, R. A., Simpson, R. W. & Reasenberg, P. A. Influence of static stress changes on earthquake locations in southern California. *Nature* **375,** 221–224 (1995).
5. Stein, R. S. The role of stress transfer in earthquake occurrence. *Nature* **402,** 605–609 (1999).
6. US Geological Survey, Southern California Earthquake Center, and California Division of Mines and Geology. Preliminary report on the 16 October 1999 M 7.1 Hector Mine, California, earthquake. *Seismol. Res. Lett.* **71,** 11–23 (2000).
7. Parsons, T. & Dreger, D. S. Static-stress impact of the 1992 Landers earthquake sequence on nucleation and slip at the site of the 1999 M = 7.1 Hector Mine earthquake, southern California. *Geophys. Res. Lett.* **27,** 1949–1952 (2000).
8. Pollitz, F. F. & Sacks, I. S. Consequences of stress changes following the 1891 Nobi earthquake, Japan. *Bull. Seismol. Soc. Am.* **85,** 796–807 (1995).
9. Pollitz, F. F. & Sacks, I. S. The 1995 Kobe, Japan, earthquake: A long-delayed aftershock of the offshore 1944 Tonankai and 1946 Nankaido earthquakes. *Bull. Seismol. Soc. Am.* **87,** 1–10 (1997).
10. Freed, A. M. & Lin, J. Time-dependent changes in failure stress following thrust earthquakes. *J. Geophys. Res.* **103,** 24393–24409 (1998).
11. Deng, J., Hudnut, K., Gurnis, M. & Hauksson, E. Stress loading from viscous flow in the lower crust and triggering of aftershocks following the 1994 Northridge, California, earthquake. *Geophys. Res. Lett.* **26,** 3209–3212 (1999).
12. Stein, R. S. & Lisowski, M. The 1979 Homestead Valley earthquake sequence, California: Control of aftershocks and postseismic deformation. *J. Geophys. Res.* **88,** 6477–6490 (1983).
13. Oppenheimer, D. H., Reasonberg, P. A. & Simpson, R. W. Fault plane solutions for the 1984 Morgan Hill, California, earthquake sequence: Evidence for the state of stress on the Calavares fault. *J. Geophys. Res.* **93,** 9007–9026 (1988).
14. Reasenberg, P. A. & Simpson, R. W. Response of regional seismicity to the static stress change produced by the Loma Prieta earthquake. *Science* **255,** 1687–1690 (1992).
15. Toda, S., Stein, R. S., Reasonberg, P. A. & Dieterich, J. H. Stress transferred by the M_w = 6.5 Kobe, Japan, shock: Effect on aftershocks and future earthquake probabilities. *J. Geophys. Res.* **103,** 24543–24565 (1998).
16. Stein, R. S., King, G. C. P. & Lin, J. Stress triggering of the 1994 M = 6.7 Northridge, California, earthquake by its predecessors. *Science* **265,** 1432–1435 (1994).
17. Jaume, S. C. & Sykes, L. R. Evolution of moderate seismicity in the San Francisco Bay region, 1850 to 1993: seismicity changes related to the occurrence of large and great earthquakes. *J. Geophys. Res.* **101,** 765–789 (1996).
18. Shen, Z. *et al.* Postseismic deformation following the Landers earthquake, California, 28 June 1992. *Bull. Seismol. Soc. Am.* **84,** 780–791 (1994).
19. Massonnet, D., Thatcher, W. & Vadon, H. Detection of postseismic fault-zone collapse following the Landers earthquake. *Nature* **382,** 612–616 (1996).
20. Savage, J. C. & Svarc, J. L. Postseismic deformation associated with the 1992 M_w = 7.3 Landers earthquake, Southern California. *J. Geophys. Res.* **102,** 7565–7577 (1997).
21. Jackson, D. D., Shen, Z. K., Potter, D., Ge, X. B. & Sung, L. Y. Geoscience: Southern California deformation. *Science* **277,** 1621–1622 (1997).
22. Bock, Y. *et al.* Southern California permanent GPS geodetic array: Continuous measurements of regional crustal deformation between the 1992 Landers and 1994 Northridge earthquakes. *J. Geophys. Res.* **102,** 18013–18033 (1997).
23. Peltzer, G., Rosen, P., Rogez, F. & Hudnut, K. Poro-elastic rebound along the Landers 1992 earthquake surface rupture. *J. Geophys. Res.* **103,** 30131–30145 (1998).
24. Ivins, E. R. Transient creep of a composite lower crust, 2. A polymineralic basis for rapidly evolving postseismic deformation modes. *J. Geophys. Res.* **101,** 28005–28028 (1996).
25. Deng, J., Gurnis, M., Kanamori, H. & Hauksson, E. Viscoelastic flow in the lower crust after the 1992 Landers, California, earthquake. *Science* **282,** 1689–1692 (1998).
26. Pollitz, F. F., Peltzer, G. & Bürgmann, R. Mobility of continental mantle: Evidence from postseismic geodetic observations following the 1992 Landers earthquake. *J. Geophys. Res.* **105,** 8035–8054 (2000).
27. Kirby, S. H. & Kronenberg, A. K. Rheology of the lithosphere: Selected topics. *Rev. Geophys.* **25,** 1219–1244 (1987).
28. Hauksson, E., Jones, L. M., Hutton, K. & Eberhart-Phillips, D. The 1992 Landers earthquake sequence: Seismological observations. *J. Geophys. Res.* **98,** 19835–19858, (1993).
29. Wald, D. J. & Heaton, T. H. Spatial and temporal distribution of slip for the 1992 Landers, California, Earthquake. *Bull. Seismol. Soc. Am.* **84,** 668–691 (1994).
30. Dreger, D. & Kaverina, A. Seismic remote sensing for the earthquake source process and near source strong shaking: A case study of the October 16, 1999 Hector Mine Earthquake. *Geophys. Res. Lett.* **27,** 1941–1944 (2000).

Acknowledgements

We thank S. Sacks for discussions and S. Keiser for computer support. This research was supported by a NSF post-doctoral fellowship and the Southern California Earthquake Center.

Correspondence and requests for materials should be addressed to A.M.F. (e-mail: freed@dtm.ciw.edu).

Emperor penguins and climate change

Christophe Barbraud* & Henri Weimerskirch

Centre d'Études Biologiques de Chizé, Centre National de la Recherche Scientifique, 79360 Villiers en Bois, France

Variations in ocean–atmosphere coupling over time in the Southern Ocean[1–3] have dominant effects on sea-ice extent and ecosystem structure[4–6], but the ultimate consequences of such environmental changes for large marine predators cannot be accurately predicted because of the absence of long-term data series on key demographic parameters[7,8]. Here, we use the longest time series available on demographic parameters of an Antarctic large predator breeding on fast ice[9,10] and relying on food resources from the Southern Ocean[11]. We show that over the past 50 years, the population of emperor penguins (*Aptenodytes forsteri*) in Terre Adélie has declined by 50% because of a decrease in adult survival during the late 1970s. At this time there was a prolonged abnormally warm period with reduced sea-ice extent. Mortality rates increased when warm sea-surface temperatures occurred in the foraging area and when annual sea-ice extent was reduced, and were higher for males than for females. In contrast with survival, emperor penguins hatched fewer eggs when winter sea-ice was extended. These results indicate strong and contrasting effects of large-scale oceanographic processes and sea-ice extent on the demography of emperor penguins, and their potential high susceptibility to climate change.

Between 1952 and 2000, the emperor penguin colony located near Dumont d'Urville Station (66.7° S, 140.0° E) in Terre Adélie was monitored continuously, generating the longest data set available on an Antarctic marine predator. Data from the meteorological station 500 m from the colony shows that, after a period of stability in the 1960s (average temperatures −17.3 °C), winter temperatures began to vary extensively and were high throughout the 1970s until the early 1980s (average −14.7 °C); they then decreased but remained variable until the present time (average −16.6 °C, $t = 3.2$, $P = 0.004$ (Student's t-test; Fig. 1a). No trend was detectable for the summer temperatures. The breeding population of emperor penguins was stable until the mid-1970s, but declined abruptly by 50% in the late 1970s and has stabilized since (Fig. 1b).

We used capture–mark–recapture data spanning 1969–1989 from ringed breeding emperor penguins to estimate adult annual survival rates (see Methods). Females survived better than males but the survival curves for males and females were parallel (additive time-dependence, see Methods; Fig. 2a). Survival was particularly

* Present address: Tour du Valat, Le Sambuc, 13200 Arles, France.